Dynamic Response of Single Electrode Conductivity Probes in Slow Flows

WILLIAM F. SIMMONS

POB 412, Woods Hole, MA 02543

BARRY R. RUDDICK

Department of Oceanography, Dalhousie University, Halifax, N.S. B3H 4J1

(Manuscript received 2 September 1983, in final form 16 November 1983)

ABSTRACT

Four designs of single electrode conductivity probes, three of them new, were tested for response characteristics in conditions simulating laboratory internal wave flows. Two of the new designs were shown to be significantly superior in sensing vertical motion without deleterious time lags. Amplitude and phase lag, and inherent nonlinearity of response are evaluated quantitatively for all designs.

1. Introduction

The conductivity at a point in an aqueous electrolytic solution can be conveniently measured using the so-called single-electrode probe introduced by Gibson and Schwarz (1963a) to monitor temperature and/or concentration of dynamically passive constituents (tracers) in a decaying turbulent flow (Gibson and Schwarz 1963b). The single electrode method places a tiny electrode (Diameter = $O(10^{-1})$ mm) in the fluid at the location where measurements are to be made. A second much larger electrode is positioned elsewhere in the fluid at a location which does not interfere with the flow. Current lines between the two electrodes converge at the smaller electrode where most of the electrical resistance occurs approximating, therefore, a point measurement. The overall circuit resistance is approximately inversely proportional to the conductivity in the immediate vicinity of the smaller electrode. For spherical geometries, more than 95% of the measured resistance is encountered within 10 electrode radii of the smaller electrode.

Geophysical fluid scientists have adopted the probes as sensors of vertical displacement in laboratory studies of unsteady laminar stratified fluid flows and internal wave studies. Typically, a laboratory tank is filled and density-stratified using salinity (NaCl) concentration or temperature gradients. Common stratifications are (i) linear (Oster, 1965) or (ii) two-layered with diffusing interface (Davis and Acrivos, 1967). Two dimensional motions in a vertical plane are induced, say, by a paddle and single electrode probes are mounted on L-shaped supports, as shown in Fig. 1, and suspended in the flow. As the fluid motion ensues, surfaces of constant density, or equivalently, conductivity are advected up and down. Probe output traces of voltage versus time $C(t)$ are converted directly to time history of vertical displacement $Z(t)$ through a prescribed stratification rule $C = C(Z)$ determined through static calibrations. Caccione (1970) used this method to study reflection/intensification characteristics of monochromatic single mode plane internal waves as they encounter a shoaling region. Martin *et al.* (1972) extended the method using arrays of probes in the vertical and horizontal to determine the amplitude of individual wave modes in a developing wave spectrum evolving by a spontaneous degeneration process. Hachmeister and Martin (1974) extended the parameter ranges of that work, and tested the growth theories.

In such laboratory flows, fluid velocities are typically 1 mm s^{-1} (amplitude of 10 mm and Brunt–Väisälä frequency of one cycle per 10 seconds). Since the probe body is usually about 5 mm in diameter, Reynolds numbers for the flow about the probe body are O(1) [compared to Gibson and Schwarz's experiments where $R \approx O(10^3)$]. Thus, fluid flow about the probe is viscous, and it is therefore possible that probe output signals $C(t)$ could lag fluid displacements $Z(t)$ by a measurable margin. Indeed, data presented by both Martin *et al.* (1972) and Hachmeister and Martin (1974) are up to ±60° in error in estimating relative vertical phase of the growing wave modes. It is furthermore possible that because the sensor itself resides at the end of long cylindrical flow obstacle (Fig. 1) there could be "end effects" causing further discrepancies between $C(t)$ and $Z(t)$ and even the possibility of a nonlinear relationship between the two.

In Section 2 of this paper we show that the single electrode conductivity probes now in common laboratory use do indeed generate significant phase and amplitude errors between probe output signals and the fluid motion. These are directly attributable to viscous

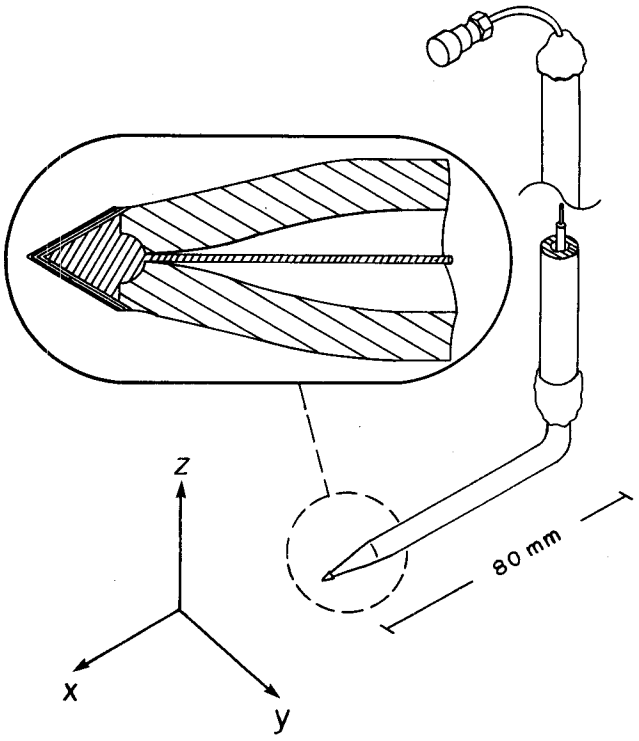

FIG. 1. The single-electrode Gibson and Schwarz (1963) blacked-platinum and glass conductivity probe as used in this study. Relative motion between the probe tip and the fluid is either vertical or in the y–z plane.

effects. In Section 3 we describe several simple corrective design alterations. In Section 4 we show results of comparative testing of all the aforementioned probe designs including evidence that all designs are somewhat nonlinear, and that the older designs can be significantly nonlinear. In Section 5 we discuss the overall convenience of the different designs and summarize results.

2. Probe response in laminar flows

The viscous nature of the Gibson and Schwarz type point probe (hereafter, GS) was confirmed by observing its response to abrupt vertical step displacements in a quiescent linearly-stratified (NaCl) fluid. Equilibrium times, $C(t)/C(\infty) = 0.95$, were commonly several minutes.

To quantify their behavior, we built a probe-oscillating "wave simulator". An electric motor, with continuously variable transmission, slowly rotated an adjustable radius eccentric arm which in turn drove, via a flexible stainless steel rope, a vertical traversing mechanism to which a probe (or probes) was rigidly attached. The maximum eccentric radius was a few centimeters and the drive cable was about a meter long so that nearly sinusoidal vertical oscillations of the probe were obtained from constant speed rotation of the eccentric. The traversing mechanism was located over a tank so that the probe tips could be positioned at an intermediate depth in the still liquid (constant Brunt–Väisälä period from 10 to 15 s). Internal waves were simulated by oscillating the probe body vertically through the quiescent fluid at periods greater than the Brunt–Väisälä period. Wake problems, if any, are maximized with this configuration since the probe traverses through the same narrow vertical column of fluid rather than distributing its wake both horizontally and vertically as would be the case in a wave field. Lag problems are also enhanced since the relative fluid velocity goes to zero at vertical displacement extremes of the probe.

Simultaneous two-frequency tests were possible using two motors with eccentrics with a simple pulley arrangement in the drive cables.

Typical responses of a platinum-tipped glass bodied GS probe to single-frequency vertical oscillations are shown in Fig. 2. The straight lines are the equilibrium probe output voltage versus vertical position. They may be regarded, to within an additive constant, as accurate representations of the equilibrium density stratification with positive z measured downward. The dots represent the maximum and minimum displacement. The oscillator is started when the tank is still. Each trace is the time variation of probe output voltage (abscissa) versus depth (ordinate) for oscillations at a single frequency. The closed path traced out after a few cycles is analogous to a Lissajous figure. In every case significant viscous lag is apparent through both amplitude underestimation and hysteresis. Note that probe response does not appear to transform with frequency in a simple way. At lower frequencies the response is a simple lag, whereas at higher frequencies the instantaneous value of $C(t)$ can occasionally lead the average value of $Z(t)$.

For one atypical large-bodied probe operated at higher frequencies, we noted that hysteresis loops such as those in Fig. 2 could be significantly closed if the probe was permitted to oscillate at fixed amplitude and frequency through many tens of cycles. However, if the oscillator were then abruptly stopped near the point of maximum velocity, an output $V(t)$ would continue at an amplitude roughly equal to the width of the original loop and at the frequency of the forced motion. We attribute that behavior to internal wave generation by the probe itself. Once a sympathetic in-phase equilibrium wave system is established in the test tank, relative speeds between the probe and the fluid are diminished in the region of maximum velocity thus flattening the width of the loop. This property was corrected by minimizing the outer diameter of probe support structures within the limits of other design constraints, and by placing wave absorbing material near the tank walls. Outer diameters of about 3 mm are the maximum allowable value in this study for wave generation to remain less than probe resolution. This limit is maintained throughout unless otherwise noted.

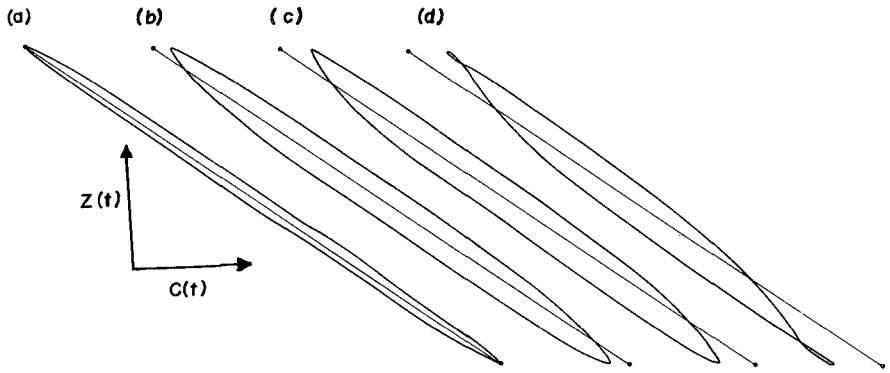

FIG. 2. Response [$C(t)$ versus $Z(t)$] of the Gibson–Schwarz probe to sinusoidal vertical displacement in a linearly stratified salt solution of buoyancy period ~9 s. The displacement amplitude is 9 mm, and the periods of oscillation are (a) 566 s, (b) 70 s, (c) 19 s, and (d) 9.3 s. The straight lines represent the equilibrium stratification and the dots denote equilibrium values of displacement extremes. Amplitude underestimation, phase lag, and nonlinearity are apparent.

3. Corrective designs

a. The flushing probe

A number of flushing probes were developed and tested during the course of this work. The one discussed here (hereafter, F) was chosen because 1) it works, 2) its fabrication requires no extraordinary facilities or materials beyond those usually available at research institutions, 3) we were able to fabricate the probes ourselves using off-the-shelf materials with the exception of one part, the probe body, which was turned on a lathe by a professional machinist and 4) once built, the probes are easy to handle and maintain.

Basically, the probe is a small hollow tube through which the laboratory fluid is continuously withdrawn by a throttled vacuum device. The sensing element is inside the tube near the inlet end and is positioned diametrically across the tube so that it is continuously flushed by the exhaust stream.

The probe housing (see Fig. 3) is a 1 mm diameter hollow plexiglass (acrylic) tube drilled diametrically near the end with a 1/4 mm hole. This part can be drilled and turned by a machinist in a few hours. Its dimensions were set as the lower limit for overall hand-held construction. The sensor itself is a 1 mm length of 0.01-inch platinum wire. It is gold soldered at a right angle to a length of 0.002 inch platinum wire and mounted diametrically across the hollow tube in the holes provided and held fast with commercial epoxy. The 0.002-inch platinum lead is then run tightly along the exterior of the tube in any convenient configuration. Once separated from the tip by a few centimeters, it is soldered to ordinary Number 40 UNC NYLCLAD copper transformer wire ($d \sim 0.0035$ inch). The exterior platinum wire and solder joint are then insulated and water proofed by painting with any convenient coating such as krylon or epoxy. The L-joint where the sensor is attached to the vertical support tube is stiffened by a small strut. With a reasonable amount of practice the above operations can be carried out with hand-held tools under a 30× laboratory microscope in a few hours time.

It remains only to mount the tip on a convenient structure that 1) preserves a continuous fluid path from probe tip to terminus, 2) insulates and water-proofs all electrical conduits, 3) provides a suitably rigid structure and 4) that is itself a minimal obstruction to the exterior flow. A number of designs are possible.

The platinum sensing element is platinum-blacked by cleaning it chemically and mechanically (chromic acid in an ultrasonic vibrator), immersing it in a 3%

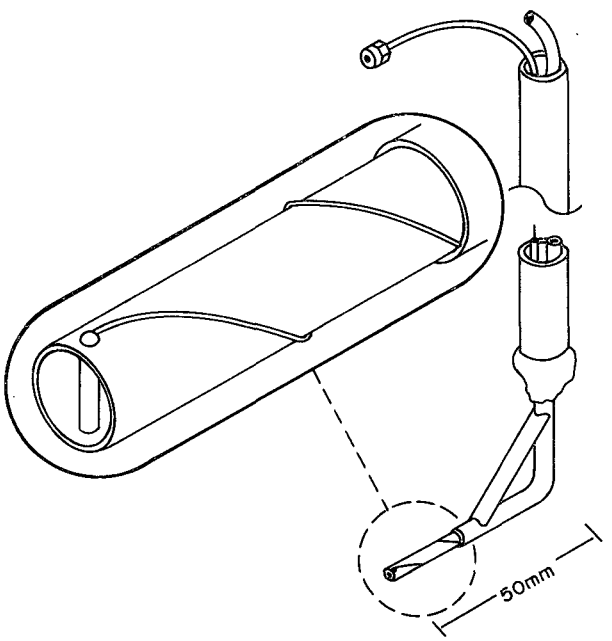

FIG. 3. The single-electrode, blacked platinum and acrylic tube flushing probe used in this study, and described in the text.

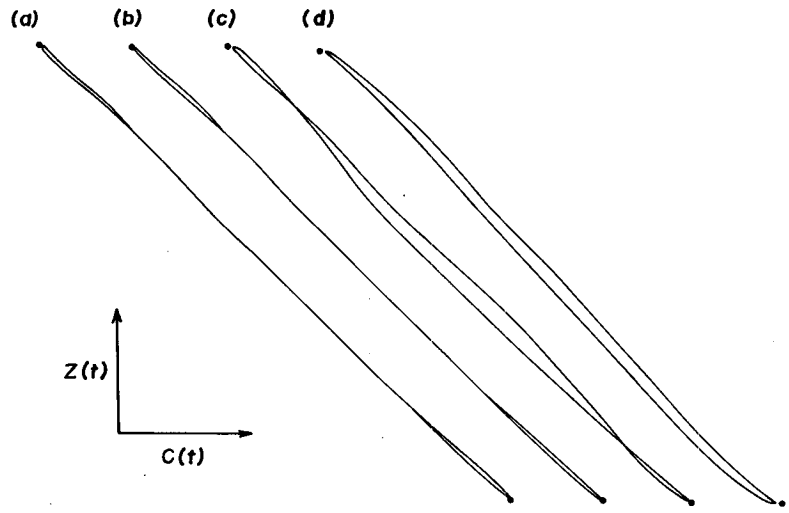

FIG. 4. Response of the flushing probe to sinusoidal vertical displacement in a linearly stratified salt solution. The amplitude is 9 mm, and the periods of oscillation are (a) 253 s, (b) 70 s, (c) 19.1 s, and (d) 9.3 s. The flushing rate is 33 $mm^3\ s^{-1}$. Compare to Fig. 2.

solution of chloroplatinic acid marketed for this purpose and subjecting it to an ac (0.07 Hz) current of a few milliamperes (Jones and Christian, 1935; Riley and Rae, 1944).

When in use, the sensing element is continuously flushed by an exhaust flow through the hollow probe body, (Fig. 3). The flow rate must be sufficient to overcome sluggish response, yet slow enough to rule out both cavitation and significant erosion of the ambient density stratification. Fortunately, a wide variety of flushing rates is possible, and in this work constant flow rates of the order of one liter per day were adequate.

Figure 4 shows the response of a flushing probe for simulated waves similar to those of Fig. 2. Note that compared to a GS probe the amplitude underestimation is almost totally absent, and that the small amounts of hysteresis that do occur sometimes correspond to lagging and sometimes to leading. Leading arises because the exhaust flow is pressure driven (i.e., the partial vacuum). The external fluid is moving around the probe body in an $R \sim O(1)$ flow and therefore has a Bernoulli-like pressure distribution around the body of the probe (cf. Batchelor, 1967, Fig. 4.12.4). This distribution contributes, in part, to the overall drag, so that high pressure is on the upstream side. The differences between that distribution and the imposed partial vacuum forces the flushing fluid past the sensor. But that pressure differential is greatest in the upstream direction, extracting slightly more upstream than downstream fluid, and therefore appearing to anticipate or lead the correct signal. The tendency to lead can be balanced by regulating the overall flushing rate so that slight leading occurs during periods of low velocity and slight lagging occurs during high velocity. That is the case in Fig. 4c.

b. The vibrating probe

The vibrating probe, (called V) is a modified GS design in which 1) the drawing of the glass tubing at the probe tip is much exaggerated, and 2) the electrode at the tip is beaded (and therefore several times larger in diameter than the platinum wire from which it is formed) rather than ground to a sharp point. In the work here, a tube of 3 mm OD lead glass was drawn to a 6 mm long tapered tip. A 0.12 mm OD platinum wire was inserted through the tip, melted back to form an exterior ball approximately 0.5 mm diameter, the ball drawn back tight against the tapered tip and the tapered glass sheath shrunk by melting to form a waterproof seal (Fig. 5).

The electrode was platinum-blacked, the glass tube bent to an L-shape, and the probe tip rigidly mounted to a hollow stainless tube of 10 mm OD.

All mechanical joints were epoxied, and the epoxy was waterproofed to prevent it from softening in the water. The drawing of the glass tip helped keep the platinum ball free of the larger structure of the probe, and its wake (see Fig. 5, insert).

Vibrating (suggested by D. Delisi) is accomplished by oscillating the stainless probe support shaft torsionally at small amplitude (0.1° angular, or 0.2 mm linear at probe tip) and at a frequency of 60 Hz. In this way a local high Reynolds number flow is superimposed on the $R \sim O(1)$ simulated wave flow. It was observed by means of dye crystals that the high frequency flow generates a slow flow which ejects water

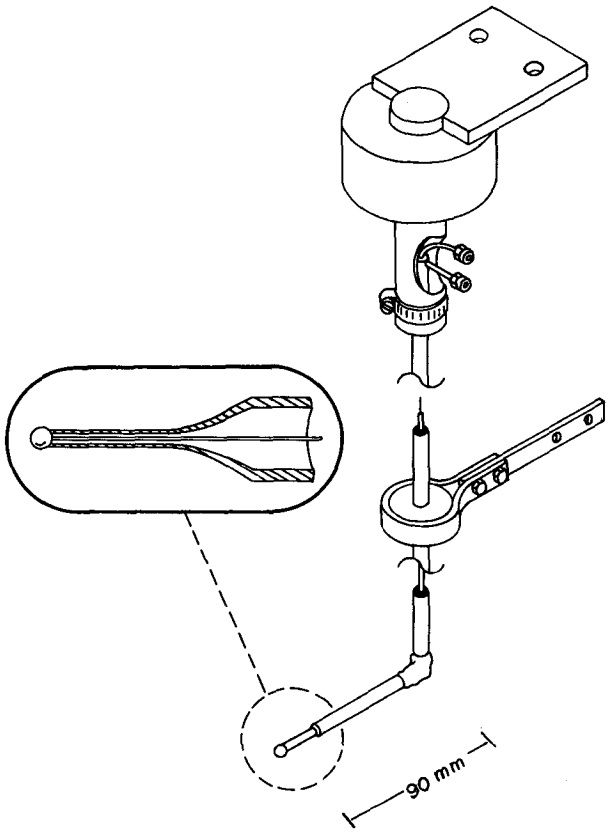

FIG. 5. The blacked-platinum and glass vibrating probe used in this study and described in the text.

laterally, thus flushing away the boundary layer from the probe tip. At larger vibration amplitudes (0.3 mm) a tendency for the signal to lead was observed. We attribute this to the same causes as for the F probe. The most satisfying dynamic results were at about 0.2 mm vibration amplitudes.

In order to cause the probe shaft to undergo torsional oscillations, the shaft of a shunt-wound 115 V dc, 1/70 H.P. motor was rigidly affixed to the upper end of the stainless probe tube. The probe shaft assembly was supported by clamping the motor housing rigidly to an external support. To prevent pendular oscillations, the lower end of the probe tube was held by a loose foam rubber grommet in a rigid clamp. The motor was caused to vibrate torsionally by applying variable voltage ac to the armature and dc to the field. These torsional vibrations resulted in horizontal 60 Hz oscillations of the probe sensing element.

c. The ceramic probe

The ceramic probe (called C) is made from commercially available ceramic tube with OD $\approx$ 0.8 mm and length of about 50 mm. A platinum wire of diameter 0.25 mm is inserted in the tube, its tip melted back to form a sphere of diameter 0.9 mm and the sphere drawn tight to the tube. The probe tip is made water tight with sealing wax, epoxy or any similar adhesive (see Fig. 6). From there, it is mounted, treated, and used like a GS probe.

4. Comparative testing

The probes were tested by moving them vertically in a salt stratification and simultaneously recording the probe displacement and probe conductivity signals. Systematic tests over a broad frequency range were performed by varying the probe position so as to provide a broad-band, pseudo-white displacement signal, with energy at all frequencies below 0.1 Hz. This was accomplished by slowly increasing the speed of oscillation from the minimum to the maximum allowed by the motor speed control. The probe transfer functions (gain and phase) were then estimated from the recorded signals. Spot checks for linearity were made by oscillating the probes at a single frequency and checking the Fourier transforms of the recorded signals for peaks at harmonics of the oscillation frequency.

a. Laboratory setup

Since vibration is known to improve probe response, the wave-simulating vertical probe motions must be very vibration-free. A probe-supporting carriage was constructed which consisted of a 5 meter long lever, pivoted at one end and free to move in a vertical plane,

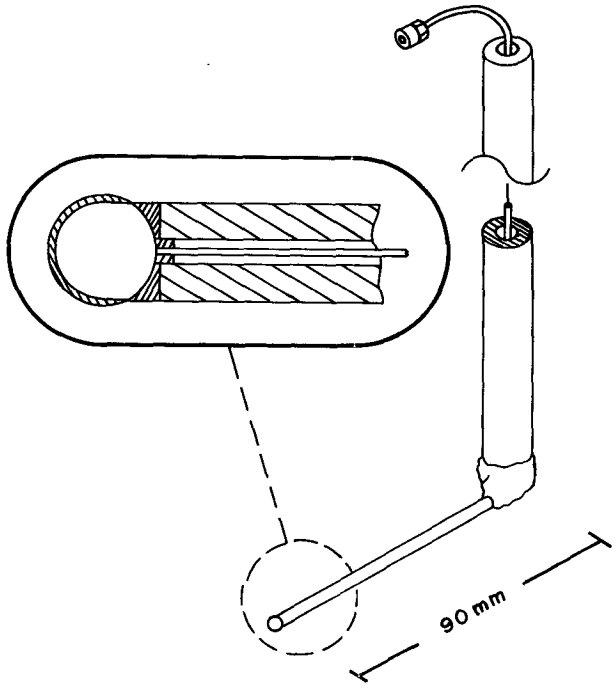

FIG. 6. The blacked-platinum ceramic-bodied probe used in this study and described in the text.

as shown in Fig. 7. The free end was attached, via a flexible, one meter long steel cable, to an adjustable radius (0–5 cm) eccentric, which was rotated by a variable speed motor. Constant speed rotation of the eccentric resulted in nearly sinusoidal and vibration-free vertical oscillations of the free end of the carriage, to which one or more probes were attached. The probe tips thus moved through the laboratory fluid very smoothly along a 5 meter radius arc. Since vertical displacements were small, a few centimeters at most, these motions were nearly linear. A simple potentiometer and pulley setup provided an accurate "Z" voltage signal representative of probe tip displacement, linear to about 0.5%.

The probe tips were suspended at mid-depth in water for which salinity increased from zero to about 2.5% in a nearly linear fashion. Over a range of 2.5 cm, the conductivity varied linearly with displacement to within about 1%. The buoyancy period was 15–20 s. The tank used was 30 cm × 183 cm and was filled to a depth of 22 cm. Wave absorbers were placed in the tank to damp out internal waves generated by the probe motions, and to ensure that the probes were moving through quiescent water, giving more accurate response measurements.

Probe conductivity was converted to analog voltage by an ac (60 kHz) bridge device, which is linear in conductivity to better than 1%. It was designed by Neil Brown (Neil Brown Instrument Systems, Inc., Catau-met, MA). The analog conductivity signals from the various probes tested and the "Z" displacement signal were low-pass filtered to avoid aliasing problems and recorded digitally on magnetic tape at two second intervals, for later analysis.

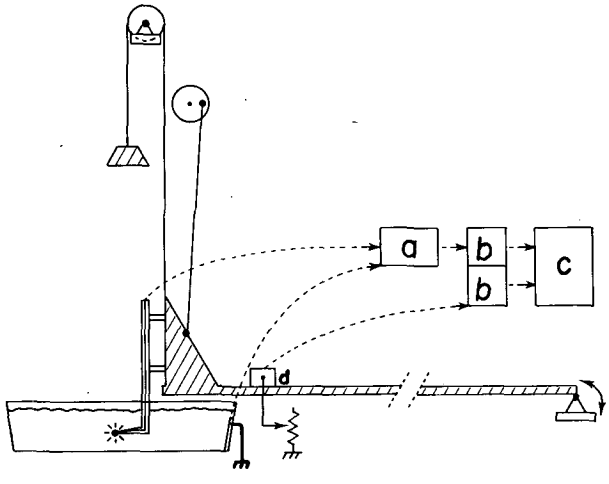

FIG. 7. Schematic diagram of the apparatus used to test the response of the conductivity probes to time varying vertical displacements. Box a is a conductivity bridge, boxes b are identical low-pass filters, box c a digital logging device, and box d generates the $Z(t)$ signal.

b. Comparative probe testing

The frequency response of a conductivity probe may be characterized by the transfer function (Jenkins and Watts, 1969), defined by

$$G(\omega)e^{i\phi(\omega)} = \frac{\hat{C}(\omega)}{\hat{Z}(\omega)}\left(\frac{dC}{dZ}\right)^{-1}, \tag{1}$$

where $\hat{C}(\omega)$ is the (time) Fourier transform of the conductivity measured by the probe, $\hat{Z}(\omega)$ the Fourier transform of the instantaneous vertical displacement of the probe, dC/dZ the conductivity gradient (assumed constant), measured by a static calibration, $G(\omega)$ is the gain of the probe at frequency ω, normalized by the gain at zero frequency, $G(0) = dC/dZ$, and $\phi(\omega)$ is the phase response of the probe. A negative phase means the probe response lags the displacement. The use of the above expression implicitly assumes that the relation between $Z(t)$ and $C(t)$ is linear, time invariant and without feedback; i.e., that G and θ depend only on frequency and not on the details, amplitude or time history of the signals C or Z.

We generated test samples of $Z(t)$ and $C(t)$ for several probes by causing the carriage and probes to move vertically over a small range, typically 1–2 cm, with frequency increasing slowly from zero to 0.1 Hz. The resulting "frequency sweep" time series, which have significant power at all frequencies below 0.1 Hz, were digitally Fast Fourier Transformed (Singleton, 1968) and estimates of the transfer function were formed from

$$G(\omega) \sim \left[\frac{L_{zc}^2(\omega) + Q_{zc}^2(\omega)}{L_{zz}(\omega)}\right]^{1/2}, \tag{2}$$

$$\phi(\omega) \sim \tan^{-1}(Q_{zc}(\omega)/L_{zc}(\omega), \tag{3}$$

where $L_{zz}(\omega)$ is the estimate of the power spectrum of $Z(t)$, $L_{zc}(\omega)$ the estimate of the co-spectrum between $Z(t)$ and $C(t)$, $Q_{zc}(\omega)$ the estimate of the quadrature spectrum between $Z(t)$ and $C(t)$ and ω is the frequency. Spectral averages were performed by averaging the Fourier coefficients over 5–10 adjacent frequency bands. Note that these transfer function estimates include response due to the local internal wavefield generated by the relative motion of fluid past the probe, which is most intense at frequencies near N, since the wave characteristics there are nearly vertical.

The above formulas were derived in Jenkins and Watts (1969) assuming the noise in C to be incoherent with Z, which is assumed to be measured perfectly. Jenkins and Watts give approximate error bounds in terms of the coherence between Z and C. However, if the noise is actually coherent with Z (for example, if the background noise is dominated by nonlinear effects), the coherent part of this noise is incorporated into the transfer function estimate, shifting it unpredictably. Under these conditions, more appropriate error bounds are

$$\frac{\Delta G}{G} \sim n, \tag{4}$$

$$\Delta\phi \sim \tan^{-1} n, \tag{5}$$

where n^2 is the fraction of noise power (or nonlinearity) present in the output signal, $C(t)$.

The degree of nonlinearity was estimated for each probe by oscillating the carriage sinusoidally, recording the output for at least sixty periods and computing the power spectra of the Z and C signals, which should consist of a single, very narrow peak. Nonlinearities show up as peaks at harmonic frequencies of the basic signal, and the fraction of power present in the signal as nonlinear noise was estimated from these peaks. Since this was a function of frequency and amplitude, the worst-case nonlinearity as a function of frequency at "typical" 1 cm peak-to-peak amplitudes was taken as characteristic of n in the error bound computations, Eqs. 4 and 5.

c. *Results*

The transfer functions of the probes were estimated for a single buoyancy frequency, $N = 0.37 \pm 0.03$ s^{-1}, which was chosen as a typical laboratory stratification. The buoyancy restoring force, and hence the probe response, will be different in a stratification with a different buoyancy frequency.

Figure 8 shows the transfer function estimates for each probe. Gain, normalized to one at zero frequency, is plotted at the left, and phase is plotted at the right. A negative phase corresponds to probe output lagging displacement.

The transfer function estimates for probe GS are in Fig. 8a. The results from several separate experiments are superimposed here, and the scatter of the data indicates that the estimated uncertainties (Eqs. 4 and 5) $\Delta G/G = 0.11$ and $\Delta\phi = 6°$ are reasonable. The response is relatively poor, with phase lags as great as 25° at 3 minute periods, and gain which falls off dramatically at frequencies higher than this.

As a check on the method, independent estimates of the transfer functions were obtained by oscillating the probe at a single frequency and recording the Lissajous figure, $Z(t)$ versus $C(t)$, after initial transients had died out. The gain and phase were estimated graphically, and these estimates are plotted for several frequencies as the circled data points. The two methods agreed to well within the estimated errors.

Figure (8b) shows the transfer function estimates for the flushing probe (F) as a function of volume rate of flow of water through the probe tip. The response is poor at very small flow rates, but for rates of from 15–60 mm^3 s^{-1} (0.7–3 liters per day), the gain is good except for a high-frequency roll-off. The phase response at these flushing rates is virtually perfect, being within 2° of zero at all frequencies below the buoyancy frequency. A slight lead in phase is evident at higher frequencies and is attributed to the effects of finite body size, which lead to

1) the Bernoulli pressure end effects, discussed earlier,

2) local internal wave generation by the horizontal part of the probe body. The probe body is relatively small and so, correspondingly, is the phase lead.

The vibrating probe (V, Fig. 8c) showed a dramatic improvement in response as the vibration amplitude was increased. At infinitesimal vibration amplitude, the phase lag was as large as 45°, and the gain was correspondingly small. As the vibration amplitude was increased, the response improved until the phase led by as much as 5°, and the gain was slightly greater than one. This lead, due to the hydrodynamic effects of the relatively large support structure, could be reduced to levels comparable to the F-probe by making the probe tip support structure smaller.

The transfer function for the ceramic probe is shown in Fig. 8d. The large viscous lag indicates that the inherently poor response of a GS type probe in low Reynolds number flows is not improved by a reduction in size of the probe support structure.

The degree of nonlinearity in the probe output under single-frequency sinusoidal depth variations was estimated for a few frequencies (10, 30 and 38 s periods) at amplitudes of 3 mm and 6 mm. Fig. 9 shows log–log plots of the periodograms for a typical test: sinusoidal oscillations at a period of 38 s and an amplitude of 3 mm. The amplitudes are normalized to the basic frequency peaks and the relative amplitudes of the harmonics can be read from the scale at left. The periodogram of the Z signal (9a) indicates that the motions were sinusoidal to better than 1%.

The four probes are ranked left to right in decreasing order of nonlinearity. They are also ranked in order of horizontal probe support tube diameter, (Probe C, Fig. 9e, is the smallest of all), suggesting that nonlinearity is due to the Bernoulli pressure end effects described earlier. The nonlinearities are much less severe at frequencies near or above the buoyancy frequency, where the viscous response tends to be better. The GS probe (9b) exhibited nonlinearities of 3.5–7% at 38 s periods; the V probe (9c) exhibited nonlinearities of 3.5–6% at a 38 s period, apparently independent of vibration amplitude. Note that the exaggerated drawing of the glass tip of this probe (Fig. 5) did not significantly improve the linearity of the response. The F probe was relatively nonlinear (6–7%) at flushing rates below 15 mm^3 s^{-1}, but at faster flushing rates, the probe was linear to better than 2%. This again suggests that nonlinearity is a hydrodynamic effect due to the flow around the tip support tube, since the suction at the probe tip must dominate the Bernoulli pressure differential in order to linearize the F probe response.

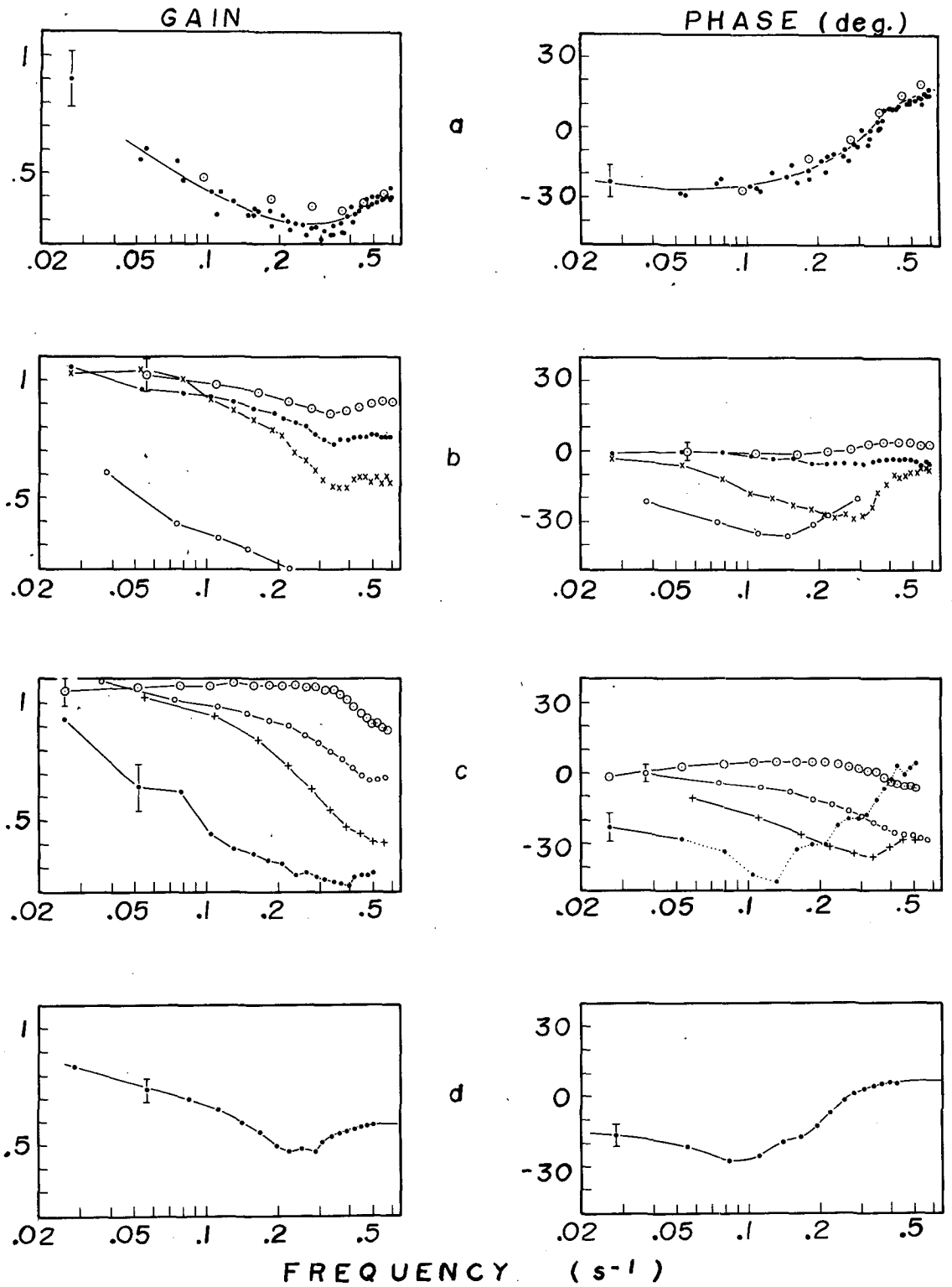

FIG. 8. Transfer functions (gain versus frequency on the left, phase versus frequency on the right) of the four probes tested. Error bars are computed from Eqs. 4 and 5. (a) Gibson–Schwarz probe response (dots) and response estimated from Lissajous figures (circled dots). (b) Response of flushing probe at a flushing rate of 67 $mm^3\ s^{-1}$ (circled dots), 15 $mm^3\ s^{-1}$ (solid dots), 3 $mm^3\ s^{-1}$ (crosses), and 0 $mm^3\ s^{-1}$ (open circles). (c) Response of the vibrating probe for a vibration amplitude of 0.33 mm (circled dots), 0.15 mm (open circles), 0.10 mm (crosses), and 0.03 mm (solid dots). (d) Response of ceramic probe.

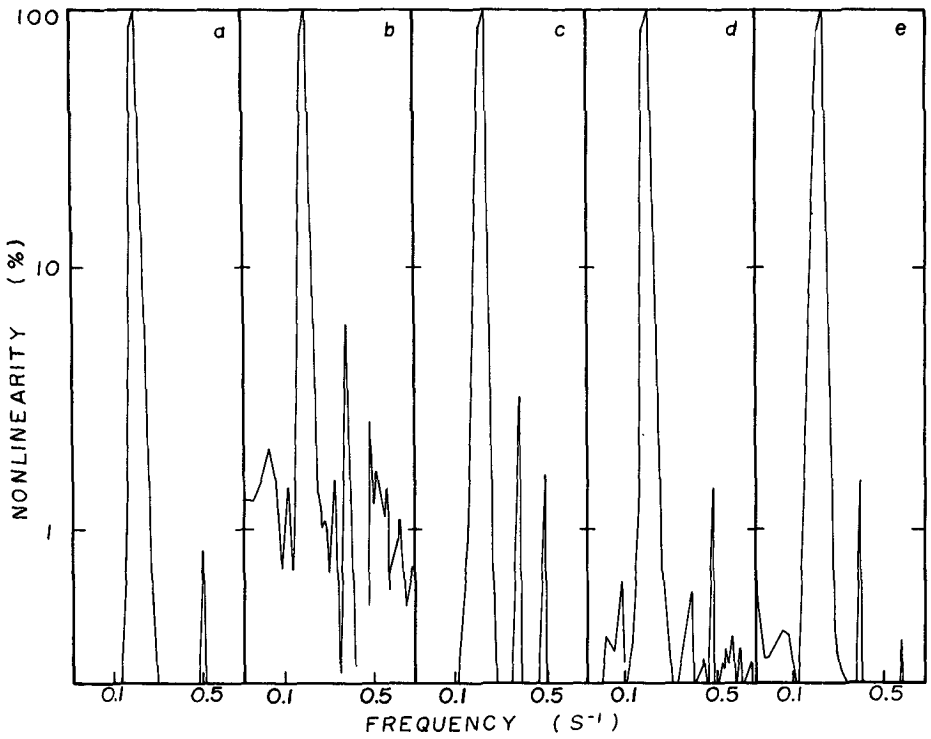

FIG. 9. Periodograms of output from probes undergoing sinusoidal vertical oscillations, amplitude 3 mm, period 38 s. The 38 s peaks have been normalized to one, and the scale at left indicates the relative amplitude (not energy) of the nonlinear harmonics: (a) "Z" displacement signal, (b) Gibson–Schwarz probe, (c) Vibrating probe, vibration amplitude = 0.11 mm, (d) Flushing probe, 3 ml min^{-1}, (e) Ceramic probe.

5. Conclusions

All the probes were easy to use, but each was found to have advantages and shortcomings which tend to make one probe more suitable than another in any particular situation. For conductivity measurements of phenomena with a time scale greater than about five minutes, the basic Gibson–Schwarz probe is adequate, although care must be taken to minimize drift problems. For measurements of laminar phenomena which have timescales shorter than this, and with no steady fluid flow past the probe tip to flush the boundary layer, either the flushing or the vibrating probe will give good performance.

The flushing probe approaches nearly perfect dynamic response and exhibits very small (0.2%) nonlinearity at moderate flushing rates. The price for this is twofold:

1) The probe is the most difficult to fabricate of those tested.

2) It has a fairly large cell constant, meaning that the electronics sees a relatively high resistance through the probe tip and must be correspondingly more sensitive. This is not a severe problem with present day electronics technology.

The vibrating probe is a very simple modification which may be applied to improve the viscous lag response of already existing, or comparatively easily fabricated, L-shaped Gibson–Schwarz type probes. The modification may be performed in a few hours. However, if the horizontal probe tip support is greater than 1–1.5 mm in diameter, two response problems associated with this structure will remain: 1) a phase lead of 5–7° at most frequencies, due to local wave generation, and 2) a nonlinearity in response of 3–6%. Normally, this amount of nonlinearity is not important, but in some uses, (such as resonant wave interaction experiments) it is important to be sure that a spectral peak at sum and difference frequencies of the basic waves is not due to the nonlinearity of the measuring instruments. The nonlinearities of the vibrating probe response can be improved by making the tip support as miniscule as possible.

Both the flushing and vibrating probes can in principle disturb the mean stratification either by removing or mixing the water in the immediate vicinity of the probe. However, rudimentary tests in a 42 × 42 cm tank linearly stratified to a depth of 10 cm, indicate that the flushing and mixing processes are slow enough that alterations to the basic stratification remain smooth and large scale (i.e., local changes are efficiently diffused over the entire depth of fluid).

The easily fabricated but fragile ceramic probe, with its sensing element at the end of a long, thin ceramic

tube, exhibits a large viscous lag. It is, however, extremely linear in response. It is conjectured that the ceramic probe would exhibit very nearly perfect response when vibrated. A variety of circumstances, one of which was the fragility of the ceramic tubing, prevented systematic testing of this probe under torsional vibration.

Acknowledgments. We are grateful to Richard Scotti who fabricated some of the equipment and participated in the early stages of experimentation, to Neil Brown who designed the probe circuitry, and to Don Delisi, who suggested that vibrating could improve probe response. This work was supported by Office of Naval Research Grant N00014-66-C0241 and was conducted at the Woods Hole Oceanographic Institution.

REFERENCES

Batchelor, G. K., 1967: *An Introduction to Fluid Dynamics,* Cambridge University Press, 615 pp.

Caccione, D. A., 1970: Experimental study of internal gravity waves over a slope. Ph.D. thesis, Massachusetts Institute of Technology and Woods Hole Oceanographic Institution, WHOI Rep. No. 70-6, 226 pp.

Davis, R. E., and A. Acrivos, 1967: The stability of oscillatory internal waves. *J. Fluid Mech.,* **30,** 723–736.

Gibson, C. H., and W. H. Schwarz, 1963a: Conductivity fluctuations in a turbulent flowfield. *J. Fluid Mech.,* **16,** 357–364.

——, and ——, 1963b: The universal equilibrium spectra of turbulent velocity and scalar fields. *J. Fluid Mech.,* **16,** 365–384.

Hachmeister, L. E., and S. Martin, 1974: An experimental study of the resonant instability of an internal wave of mode 3 over a range of driving frequencies. *J. Phys. Oceanogr.,* **4,** 337–348.

Jenkins, G. M., and D. G. Watts, 1969: *Spectral Analysis and Its Applications,* Holden-Day, 525 pp.

Jones, G., and S. M. Christian, 1935: The measurement of conductivity of electrolytes: On platinization. *J. Amer. Chem. Soc.,* **57,** 280–284.

Martin, S., W. F. Simmons and C. I. Wunsch, 1972: The excitation of resonant triads by single internal waves. *J. Fluid Mech.,* **53,** 17–24.

Oster, G., 1965: Density gradients. *Sci. Amer.,* **213,** 76.

Riley, J., and W. N. Rae, 1944: *Physical Chemical Methods,* Vol. I. D. Van Nostrand, 433–434.

Singleton, R. C., 1968: An algorithm for computing the mixed radix fast fourier transform. Mathematical and Statistics Division, Stanford Research Institute.